International Academic Institute for Science and Technology

International Academic Journal of Science and Engineering
Vol. 13, No. 2, 2026, pp. 26-40.

ISSN 2454-3896

International Academic Journal of Science and Engineering

www.iaiest.com

An Inverted L-Stub Shaped Multiband Antenna for IoT and Military Communication Applications

A. Rajagopal [a], K. Jyostna [b], Narra Dhanalakshmi [c], V. Lokesh Raju [d], G. Srinivasa Rao [e], B.T.P. Madhav [f*]

[a] Antennas & Liquid Crystals Research Centre, Department of Electronics and Communication Engineering, Koneru Lakshmaiah Education Foundation, Andhra Pradesh, India. E-mail: akellaraj@gmail.com, Orcid: https://orcid.org/0009-0006-1824-1648

[b] Department of Electronics and Communication Engineering, VNR VJIET, Hyderabad, India. E-mail: jyostna_k@vnrvjiet.in, Orcid: https://orcid.org/0000-0003-0669-5897,

[c] Department of Electronics and Communication Engineering, VNR VJIET, Hyderabad, India. E-mail: dhanalaksmi_n@vnrvjiet.in, Orcid: https://orcid.org/0000-0003-0439-9365

[d] Associate Professor, Department of Electronics and Communication Engineering, Aditya Institute of Technology and Management, Tekkali, Srikakulam, Andhra Pradesh, India. E-mail: vlokeshraju@gmail.com, Orcid: https://orcid.org/0000-0002-9196-0765

[e] Antennas & Liquid Crystals Research Centre, Department of Electronics and Communication Engineering, Koneru Lakshmaiah Education Foundation, Andhra Pradesh, India. E-mail: srinivas.bharadwaja@gmail.com, Orcid: https://orcid.org/0009-0007-6516-2130

[f] Antennas & Liquid Crystals Research Centre, Department of Electronics and Communication Engineering, Koneru Lakshmaiah Education Foundation, Andhra Pradesh, India. E-mail: btpmadhav@kluniversity.in, Orcid: https://orcid.org/0000-0002-6893-6978*

Abstract

A compact, inverted L-stub multiband antenna measuring 21x16x1.6 mm^3 was constructed on Rogers 5880 substrate. The antenna is made to work with smart devices that need to connect to the IoT, 5G networks, and aeronautical mobile telemetry (AMT) applications. The proposed model provides bandwidths of 170 MHz (4420 to 4590) MHz, 890 MHz (5010 to 5900) MHz, and 120 MHz (5740 to 5860) MHz. The proposed antenna exabits a wide bandwidth of 10 dB from 4.42 - 4.59 GHz, 16.3% from 5.01 to 5.90 GHz, and 2.01% from 5.74 - 5.86 GHz, offers a peak gain of 6.81 dBi at 5.7 GHz, an average efficiency of 83.2%, and it also operates at 4.48 GHz & 5.04 GHz.

Keywords: Aeronautical Mobile Telemetry (AMT), Internet of Things (IoT), L-Stubes, Multiband.

DOI: 10.71086/IAJSE/V13I2/IAJSE1351
Received: 21 February 2026/Revised: 02 April 2026/Accepted: 05 May 2026/Published: 30 June 2026

Introduction

Aeronautical Mobile Telemetry (AMT) enables the real-time transmission of flight-test and performance data from airborne platforms to ground stations under high-dynamic operating conditions. It supports continuous monitoring of aerodynamic, structural, propulsion, and avionics parameters, ensuring operational safety and system reliability. Modern aeronautical mobile telemetry (AMT) systems use better modulation methods, strong error-control techniques, and properly designed antennas. These features reduce Doppler effects, multipath interference, and signal attenuation over long distances. As a result, AMT enables reliable data collection during flight experiments. It also supports the evaluation and certification of aerospace systems.

Small devices which use minimal power connect through the Internet of Things to perform their data collection and communication duties. These devices function in different settings which enable users to watch their operations while they perform their control duties. The systems need to support multiple network nodes while they must deliver fast responses and maintain continuous operational availability. Modern IoT platforms serve as essential tools which enable wireless connectivity that operates through multiple frequency ranges while delivering broad spectrum availability. The antenna operates as the primary element which determines device performance because space restrictions affect compact device designs. The system's first factor creates an immediate effect on signal quality together with power consumption and system stability. an antenna is constructed for sub-6 GHz and microwave frequency bands need to deliver superior performance together with multiple installation methods for their broadband operational capabilities. The design process needs to solve three main challenges which include antenna dimensions and its ability to emit radiation and maintain stable electrical characteristics. The process of creating IoT antennas becomes difficult because these devices need to function with both body-worn devices and systems which need to operate directly on human skin. The system faces three core problems which include signal propagation changes and human body effects and legal restrictions. The development of compact wideband antennas stands as a vital requirement because they offer stable communication links to IoT devices

The stub-based loading method is an efficient way to modify the impedance and resonance properties of planar antennas. This technique allows for changes in electrical length without requiring any physical enlargement of the device. The presence of stubs in the current path introduces small reactive components, leading to shifts in operating frequencies. Designers employ open and short stubs to create multiple resonance frequencies, aiding in the development of wideband and multiband systems. The system components collaborate to suppress unwanted signal modes while enhancing the alignment between system impedance and load impedance.

The integration of stubs enables engineers to enhance antenna performance through a compact design that utilizes straightforward manufacturing processes. This stub-based design strategy offers a simple solution that demands less maintenance compared to complex multilayer or active tuning systems. Properly designed stubs help reduce mismatches between feed systems and substrate-induced parasitic elements. Wireless and IoT systems rely on stub-based techniques to achieve compact designs with a broad frequency range and stable frequency performance.

A multiband antenna operates at two or more frequency bands. It allows a single device to support multiple wireless communication services. These services may include GSM, LTE, Wi-Fi, GPS, Bluetooth, and 5G communication systems. Multiband operation is achieved by creating different resonant paths at selected frequencies. This is commonly done using slot structures, meandered lines, fractal geometries, or parasitic elements in the antenna layout. Every path is tuned to a desired frequency, creating a few desired frequency bands with low return loss and excellent VSWR. This integration saves space and makes the system easier to use by combining several wireless functions into a single and compact unit.

The fig. 1 gives a broad summary of the different applications in frequency spectrum of 2 to 6 GHz, which is critical to modern satellite, radar, and wireless technologies. The ISM applications, medical telemetry & Wireless Body Area Networks (WANs) are popularly used in the lower frequency range (2.0 to 2.5 GHz). High-capacity, including 4G Long Term Evolution, WiMAX, and 5th Generation New Radio (5G NR, n41, C-band), supports the mid-range frequency band (2.5 - 4.5 GHz). This spectrum has other applications, such as military and defence, radar, satellite communications, and fixed wireless access. All these frequency bands are critical to next-generation communication, defence, and remote sensing technologies.

Previous studies have reported compact and wearable antenna designs for vehicular and body-area communication systems (Sai et al., 2022; Li et al., 2022). In Sai et al., (2022), a compact antenna on an FR-4 substrate is developed for DSRC-based vehicular communication near 5.9 GHz, showing satisfactory impedance bandwidth, gain, and radiation performance for road safety applications. In Li et al., (2022), a flexible textile antenna using a slotted circular

patch is fabricated on a denim substrate with conductive fabric and dimensions of 60 × 60 × 1.17 mm³. It operates in the ISM, WiMAX, & sub-6 GHz 5G bands, maintains stable resonance under bending, exhibits low SAR values, and provides improved gain and bandwidth for wearable communication use. Several studies have reported compact multiband antennas for portable, wireless, and medical applications (Hussain et al., 2022; Mahendran et al., 2021; Shah et al., 2024).

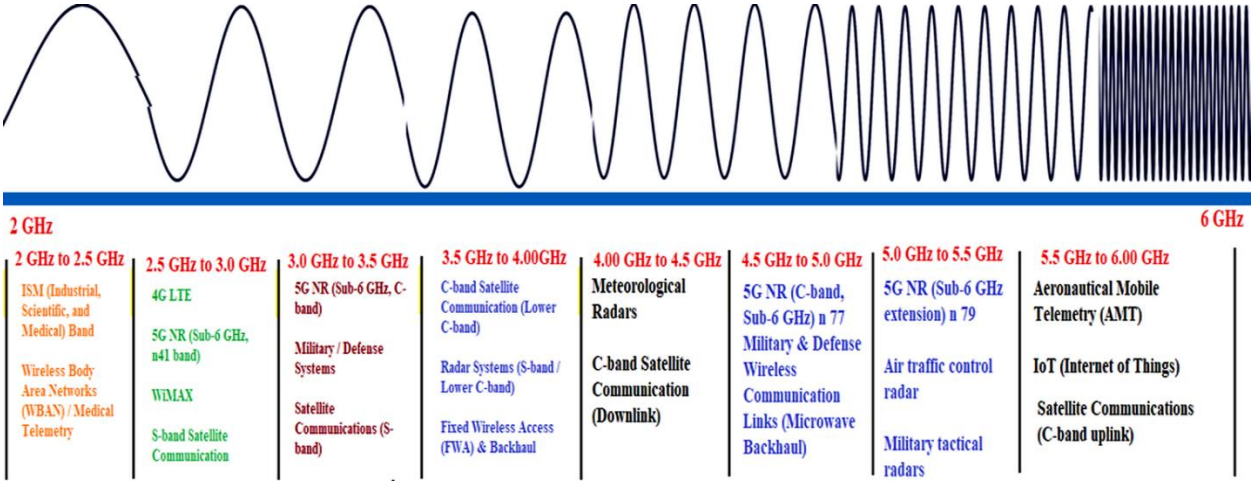


Fig. 1: Applications of the Frequency Spectrum Between 2 – 6 GHz

In Hussain et al., (2022), a reconfigurable antenna using a slotted circular patch, a rectangular stub, and a PIN diode is presented, which operates from 2.76 to 8.21 GHz in the ON state and at 2.45/5.8, 5.2, and 8 GHz in the OFF state, with gains ranging from 2.49 to 5.8 dBi and stable performance under bending. In Mahendran et al., (2021), a quad-band triangular microstrip antenna with a split ring resonator and slot structures is reported for WLAN, WiMAX, and C- and X-band applications, operating at 3.5, 4.1, 5.6, and 9.7 GHz with improved bandwidth and gain. In Shah et al., (2024), a miniaturized implantable antenna of 0.7 mm³ is designed for medical devices, operating at 915, 1450, 1900, and 2450 MHz, showing stable performance in body models, bandwidths of about 136–134 MHz, gains from −27.45 to −22.48 dBi, and reliable communication up to 2.5 m for IIoMT use. Several studies have reported advanced antenna designs for wearable, full-duplex, wideband, and multiband applications (Samal et al., 2022; Rana et al., 2024; Ranjan & Kumar, 2021; Angadi et al., 2024; Viswanadha & Raghava, 2021). In Samal et al., (2022), a wearable textile antenna with a full ground plane is developed for WBAN use, operating at 2.45 and 5 GHz with an average gain of about 7.2 dBi. In Rana et al., (2024), a compact planar full-duplex antenna using dual resonant modes and a parasitic strip achieves high isolation above 30 dB and operates from 5.95 to 6.47 GHz with a peak gain of 8.2 dBi. In Ranjan & Kumar, (2021), an ultra-wideband filtering antenna with a stepped patch and inverted T-shaped filter covers 3 to above 14 GHz, with a notched band at 5.55–6.98 GHz and a maximum gain of about 6.8 dBi. In Angadi et al., (2024), a stub-loaded antenna with dumbbell meta-atoms operates at 2.445, 5.85, and 8.83 GHz, provides circular polarization from 5.15 to 5.63 GHz, and achieves gains up to 4.36 dBi. In Viswanadha & Raghava, (2021), a compact oval-ring antenna with folded meander lines and L-shaped stubs covers the C to K bands at 6.21, 9.4, 16.78, and 25 GHz, with a maximum gain of about 8.1 dBi, efficiency above 60%, and circular polarization at 16.78 GHz. Several studies have reported compact and multiband antenna designs for wireless and 5G applications (Kumar et al., 2023; Khan & Nokerov, 2021; Chung et al., 2024; Noor et al., 2023; Faris & Tulu, 2024; Lavadiya et al., 2022). In Kumar et al., (2023), a tri-band monopole antenna with a partial ground and three inverted L-shaped stubs operates at 2.4–2.52, 3.4–4.1, and 5.2–6.6 GHz on an FR-4 substrate, achieving a peak gain of about 3.8 dB. In Khan & Nokerov, (2021), a fan-stub slot patch antenna is optimized for CBRS use by analyzing stub size with return loss and VSWR, supporting LTE-43, LTE-48, and the 5.5 GHz WLAN band. In Chung et al., (2024), a compact multiband antenna for 4G LTE, sub-6 GHz, and WLAN devices is fabricated on FR-4 with dimensions of 70 × 12.5 mm and provides a gain of about 5 dBi with good isolation and efficiency. In Noor et al., (2023), a slot-loaded patch antenna with parasitic strips on FR-4 supports 5G n77, n78, and n96 bands and offers bandwidths of about 160 MHz at 3.45 GHz and 220 MHz at 5.9 GHz. In Faris & Tulu, (2024), a multiband patch antenna with slots and defected ground on RT/Duroid 5880 covers the C, X, Ku, K, and Ka bands from 1 to 40 GHz with a size of 20.27 × 16.76 × 1 mm³. In Lavadiya et al., (2022), a frequency-tunable antenna using two PIN diodes on FR-4 operates in the S, C, X, and Ku bands, provides four tunable bands with a range of about 700 MHz, and achieves a minimum return loss of −28.22 dB. Several studies have reported multiband and specialized antenna designs for wireless, wearable, medical, and 5G applications (Kaur & Malik, 2021;

Wa'il et al., 2022; Verma et al., 2024; Sharma et al., 2024; Abutarboush, 2022; El-Hakim & Mohamed, 2023; Wang et al., 2021; Shah et al., 2019; Rajkumar & Kommuri, 2018). In Kaur & Malik, (2021), an elliptical fractal antenna on Rogers RT/Duroid 5880 operates at 2.6, 6, and 8.2 GHz with good gain and wide bandwidth for WBAN, ISM, S-, and X-band use. In Wa'il et al., (2022), a double annular-ring antenna with six sectors covers Ku-, K-, and Ka-bands at 13.10, 20.72, 25.00, and 28.85 GHz, providing bandwidths up to 2.04 GHz and gains between 6.11 and 8.31 dB. In Verma et al., (2024), a slit-loaded multiband antenna for L- and S-bands operates at 1.63, 2.0, and 2.87 GHz with high efficiency above 85% and gains up to 5 dB. In Sharma et al., (2024), a CSRR-based antenna with a cross-shaped stub supports 2.45, 3.3, and 5.8 GHz for ISM and 5G applications, with SAR values around 0.33 W/kg suitable for wearable and biomedical use. In Abutarboush, (2022), a flexible inkjet-printed antenna on synthetic paper maintains stable performance under bending and provides gains from −3 to +2 dBi with efficiency between 40% and 60% for flexible 5G devices. In El-Hakim & Mohamed, (2023), a mm-wave multiband antenna on Rogers RT/Duroid 4003 operates at 25–32 GHz and 40–60 GHz with dimensions of 24 × 24 × 0.203 mm³ and achieves a gain of about 10.75 dBi. In Wang et al., (2021), a fractal antenna on FR-4 covers 1.8–2.9, 3.4–4.6, and 5.0–5.6 GHz with gains up to 3.34 dBi. In Shah et al., (2019), a compact spiral implantable antenna operates at 402–405 MHz, 1520–1693 MHz, and 2400–2483.5 MHz with gains from −30.5 to −18.2 dBi for medical devices. In Rajkumar & Kommuri, (2018), a TCSRR-based metamaterial antenna provides multiband operation at 2.4/5.2, 2.5, 7.4, and 8.2 GHz with stable radiation patterns.

In this work, a simple antenna design was developed to enable quick simulation in CST. The antenna was developed on a copper-clad Rogers substrate & successfully operated at three different frequencies under 6 GHz. This provides an option for a single-feed tri-band antenna operating at microwave frequencies (4.48, 5.04, 5.78 GHz), which can provide 5G connectivity and support meteorological radar systems, defence, military data transmission, aeronautical mobile telemetry (AMT) applications, IoT devices, and smart sensors.

Antenna Design and Geometry

The study presents a microstrip antenna employing an inverted L-shaped stub in combination with a defected ground configuration, and provides a comprehensive analysis of the design parameters that critically affect its impedance behavior and radiation performance.

Antenna Geometry

The designed antenna is based on a triangular monopole structure with five loading stubs of different electrical lengths. The use of a 50-Ω coplanar waveguide feed is an exciting aspect of the design. To minimize the overall dimensions, the stubs are extended to the substrate. The rogers (5880) material used to fabricate the antenna with a relative permittivity of 2.2, the height of the substrate is 1.6 mm, & a loss tangent of 0.0009. The radiating element is formed using a copper layer of 0.035 mm thickness. The antenna has overall dimensions of 16 × 21 × 1.6 mm³, and each stub is 1 mm wide with a 1 mm gap between neighbouring stubs. The design & analysis are evaluated through CST Microwave Studio. The effective stub lengths are calculated using the analytical expression given in the next section.

$$\ell = \frac{c}{4f_0\sqrt{\varepsilon_{eff}}} \tag{1}$$

In equation (1), 'c' denotes the light speed in vacuum, while 'f_0'refers to the frequency at the center & is calculated using the relation given below.

$$fo = \frac{c}{\sqrt{\varepsilon eff}\,\lambda f} \tag{2}$$

In equation (2), 'ε_{eff}' represents the effective dielectric constant, & 'λ_g' denotes the guided wavelength & is calculated using the following relation.

$$\varepsilon eff \approx \frac{\varepsilon\gamma+1}{2} + \frac{\varepsilon\gamma+1}{2}\left(1+12\left(\frac{p}{h}\right)\right)^{-0.5} \tag{3}$$

In equation (3) 'ε_r' denotes the relative permittivity of the material, 'p' represents the triangular monopole width, & h indicates the height of the Rogers material.

Antenna Design Iterations

Based on mathematical analysis, several inverted L-shaped stub-loaded microstrip antennas featuring defected ground structures were designed. Fig. 2 iteration process and their performance was evaluated through iterative testing,

comparing as a function of L shapes. Four antenna iteration designs are shown, each accompanied by a reverse-side image and corresponding S_{11} and VSWR graphs from CST simulation software.

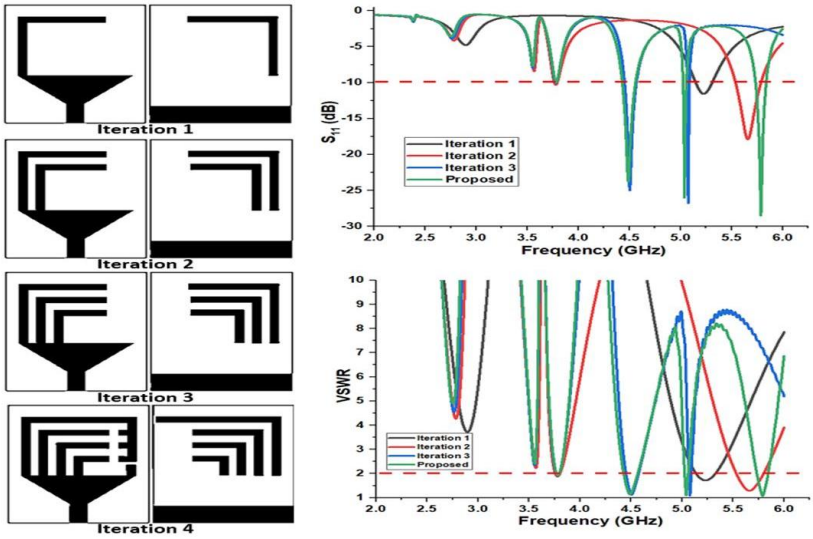
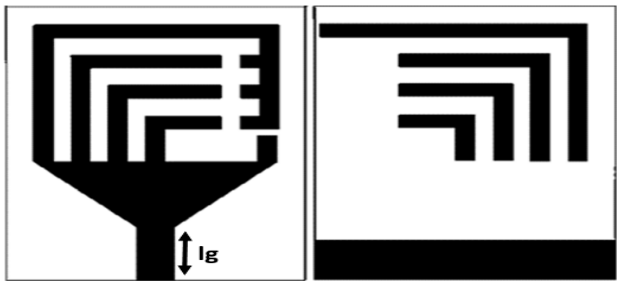


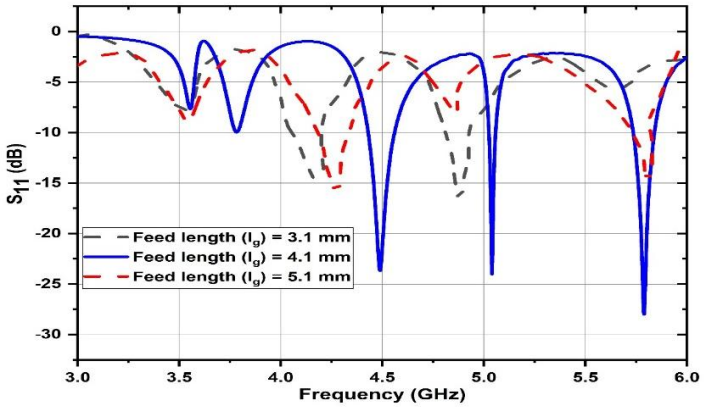
Fig. 2: Shows 4 Iterations of the Designed Antenna, and Iteration-Based Simulated Values of S11 and VSWR are Presented

Parametric Analysis

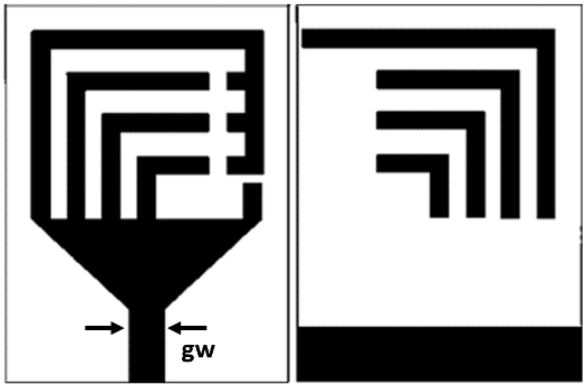
Parametric analysis is a method for examining how changes in factors such as shape, material composition, or operational frequency impact the overall system. This method changes one thing at a time and keeps the others the same. It clarifies what factors have the most significant impact on the results, such as efficacy, breadth of operations and stability. Parametric analysis will provide one with a sensitive insight into crucial variables, thus, making it easier to create stronger and more valid designs.



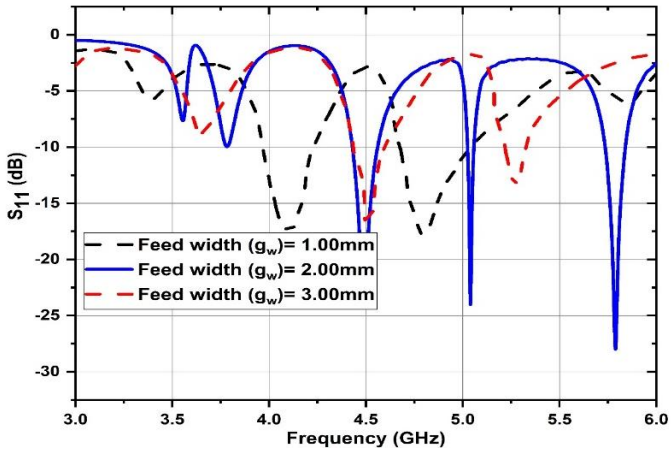
(a)



(b)



(c)



(d)

Fig. 3: Parametric Analysis of the Suggested Antenna. (a) Feed Length (lg); (b) S11 of Feed Length Variation (c) Feed Width (GW), & (d) S11 of Feed Width Variation

In fig. 3 (a) show the correlation between the feed length and the respective antenna characteristics. Fig. 3 (b) also clarifies the effect of feed length changes on the radiative characteristics, especially the return loss at the 2-6 GHz range. We find that resonance frequencies change with the increase of the feed length between 3.1mm and 5.1 mm, and the depth of the S_{11} (dB) vibrates correspondingly to the matching conditions. The 4.1mm feed length in the three illustration cases has the best impedance matching and results in a strong dip below -20 dB, which is beneficial in enabling efficient radiation, and at the same time, the reflection is reduced. Consequently, precise optimization of the feed length is essential for bandwidth enhancement, which in turn improves the overall antenna performance and enables simultaneous operation over multiple frequency bands. Fig. 3(c) presents the parametric influence of the feed-line width, whereas fig. 3(d) shows the resulting antenna response for feed widths of 1mm to 3 mm across the 2–6 GHz frequency span. The choice of feed width is observed to significantly modify the resonant behavior of the antenna and strongly affect the associated return-loss performance. Interestingly, the feed width of 2.0mm gives the best results as it has the deepest dips in the return loss at below -20dB which means that there is a minimal signal reflection & the impedance matching is excellent.Therefore, selecting the correct feed width is crucial for achieving optimal bandwidth and efficient antenna operation.

Proposed Antenna Design with Optimised Dimensions

In fig. 4, the antenna is designed to be compact in size, and shorting pins are employed to link the stubs on its opposite side. These stubs are kept to lengths that match the antenna's different resonant frequencies.

Standard design equations for microstrip antennas determined the initial antenna dimensions based on the target resonant frequency. Parametric optimization was carried out using full-wave electromagnetic simulations to improve impedance matching, bandwidth, and radiation performance. For wideband operation, the antenna uses a compact

radiating patch fed by a microstrip line with a partial ground plane. The optimized geometric parameters are presented in the next section. The corresponding structural dimensions are summarized in tables 1 & 2.

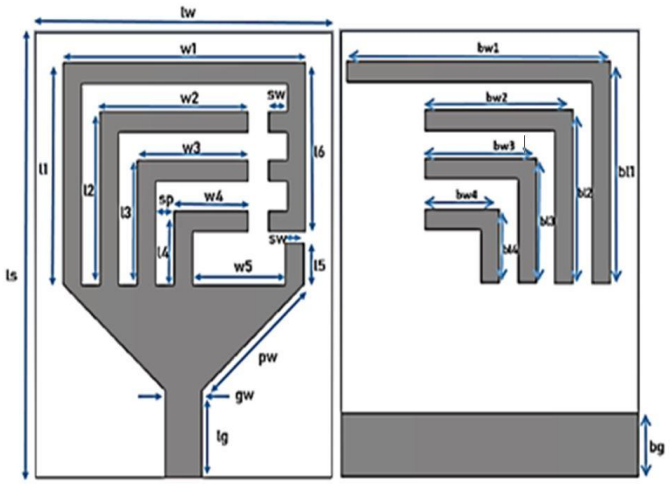


Fig. 4: Proposed Antenna Model with Representation of Dimensions

Table 1: Design Dimensional Values of the Suggested Antenna

S. No	Parameters of the Proposed Antenna Model	Value (mm)
1	Feed Length (l_g)	04.10
2	Extended length of monopole (p_w)	07.43
3	Feed width (g_w)	02.00
4	Length of stub 1 (l_1)	10.50
5	Width of stub 1 (w_1)	13.00
6	Extended length of stub 1 (l_6)	08.00
7	Extended widths of stub 1 (s_w)	01.00
8	Length of stub 2 (l_2)	08.20
9	Width of stub 2 (w_2)	08.00
10	Length of stub 3 (l_3)	05.90
11	Width of stub 3 (w_3)	06.00
12	Length of stub 4 (l_4)	03.50
13	Width of stub 4 (w_4)	04.00
14	Length of stub 5 (l_5)	02.00

Table 2: Dimensional Values for the Suggested Antenna

S. No	Parameters of the Proposed Antenna Model	Value (mm)
1	Width between stub 4 & 5 (w_5)	05.00
2	Length of substrate (l_s)	21.00
3	Width of substrate (l_w)	16.00
4	Width of stub 1 (bw_1)	14.20
5	Length of stub 2 (bl_2)	08.20
6	Width of stub 3 (bw_3)	06.00
7	Width of defect ground (b_g)	03.00
8	Thickness of Substrate	01.60
9	Thickness of Copper clad	0.035

The final model with these dimensions is evaluated using simulated S-parameters, gain, and radiation patterns. The following section provides a detailed analysis of these results.

In fig. 5 illustrates the simulated S_{11} & VSWR of the proposed antenna over the 3–6 GHz frequency range. At frequencies of 4.43, 5.04, & 5.78 GHz, the S_{11} remains below −10 dB, indicating the impedance matching and satisfactory radiation performance. VSWR indications have not exceeded the value of 2 at any point and indicate low

signal reflection and good matching between feed and patch. The proposed antenna offers wideband performance. Therefore, it is suitable for IoT applications, fifth-generation (5G) wireless devices, and aeronautical mobile telemetry (AMT) applications.

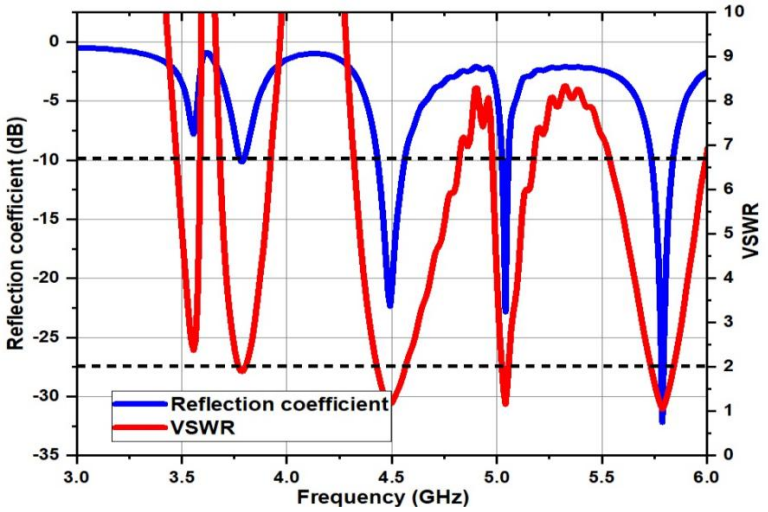
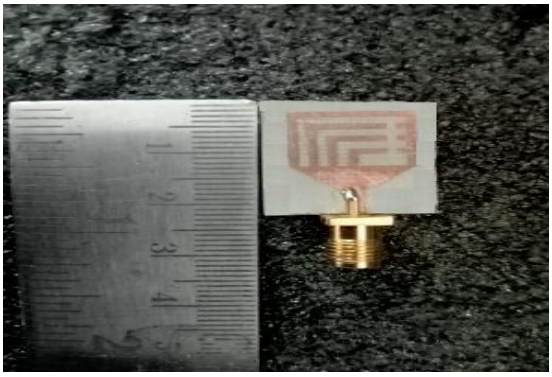


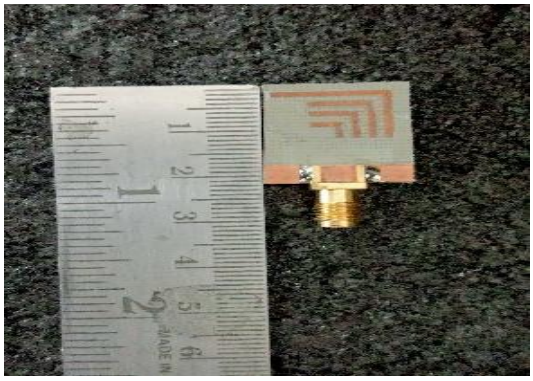
Fig. 5: Simulated Values of S11 & VSWR of the Final Antenna

Prototype of the delineated Antenna

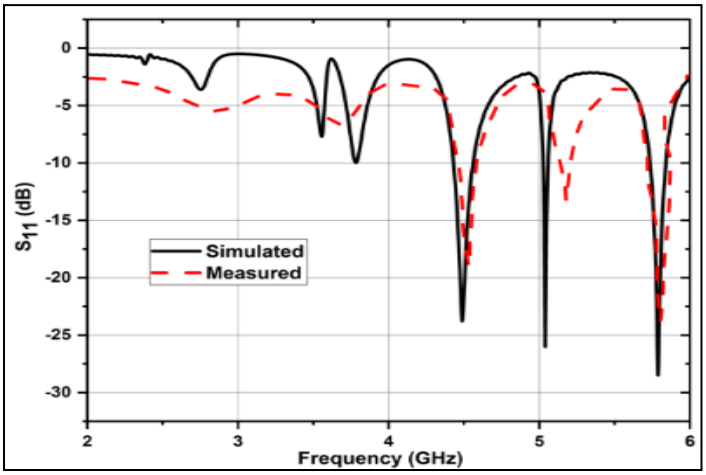
The prototype serves to assess the suggested antenna design and determine its effectiveness and dependability. The model combines both simulation outcomes and experimental performance, thereby validating the performance of antenna in a real environment. This clearly shows that the design is accurate and reliable in wireless applications, as indicated by the high correlation between the simulated & measured data.



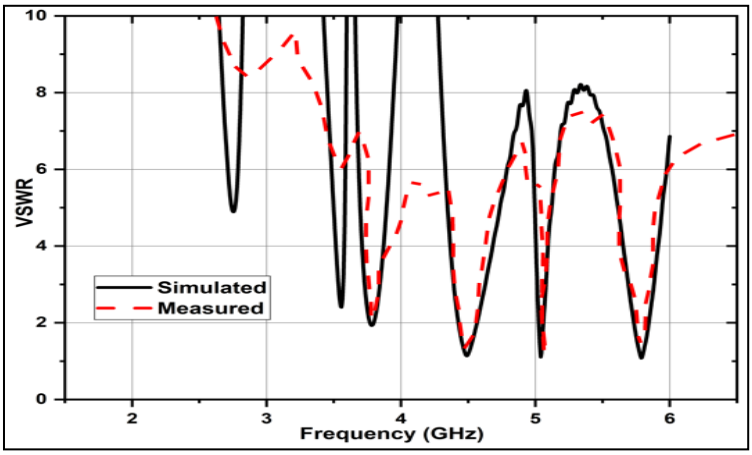
(a)



(b)



(c)



(d)

Fig. 6: Fabricated Antenna Prototype: (a) Front View, (b) Rear View, (c) & (d) Simulated & Measured Comparison of S11 &VSWR.

In fig. 6(a) and (b) display the constructed prototype of the suggested antenna, illustrating the front and rear perspectives, respectively. an antenna was prototyped by a Roger material. To achieve wideband performance, the radiating patch was designed with an altered geometry. A SMA connector of 50-Ω was attached at the feed point to facilitate precise measurements using a Vector Network Analyzer. A reference scale is placed near the antenna to show its compact size. This confirms that the antenna is suitable for portable and highly integrated wireless devices. Fig. 6(c) and (d) compares the simulated & experimentally obtained S_{11} characteristics of the proposed antenna, where both responses remain below −10 dB over multiple frequency regions, indicating excellent impedance matching and wide operating bandwidth. This minor discrepancy between the simulated & calculated results is because of the minor difference in fabrication & measurement which proves that the antenna is reliable when it comes to communication. The measurements were correct and gave the real frequencies of 4.43, 5.04, and 5.78 GHz, which agree with the simulated frequencies. This validates that the antenna is capable of use in various bands in small gadgets.

Radiation Pattern Measurement Setup

Anechoic chambers are highly engineered laboratory settings that are used to testing an antenna to measure the radiation characteristics with the highest level of precision. Through reducing the confounding effect of reflected waves, an open-space illusion is created, it is made possible by placing radio-frequency (RF) absorbing materials on all the interior surfaces (see fig. 7). A calibrated standard gain horn antenna (2 to 18) GHz covering the operating frequency band was used as the reference antenna for radiation and gain measurements. In this type of controlled environment, the primary antenna parameters, i.e., radiation pattern, gain, and directivity are measurable without extraneous perturbations. The results of these chambers are credible, repeatable standards which are accurate

reflections of the actual performance of an antenna in the open environment. As a result, anechoic chambers have continued to be invaluable tools of measuring with a high degree of rigor the energy radiation efficiency of future antenna designs. In a completely anechoic chamber, far-field radiation was measured with the test antenna placed 2 meters away from a calibrated reference antenna. This distance satisfies the far-field requirement ($R \geq 2D^2/\lambda$) based on the maximum antenna dimension (21 mm) and the highest operating frequency of 5.78 GHz.

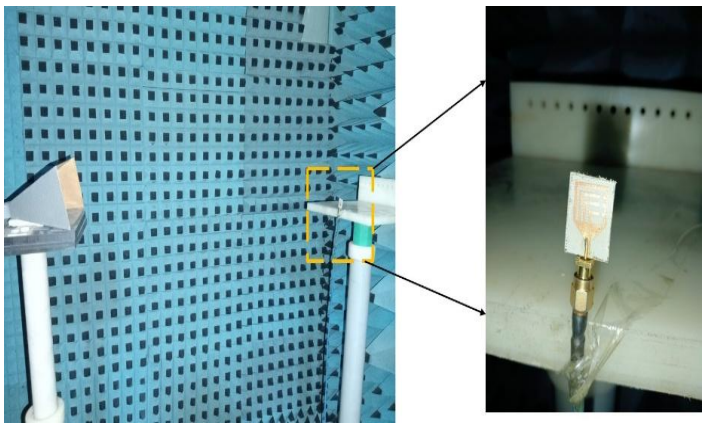
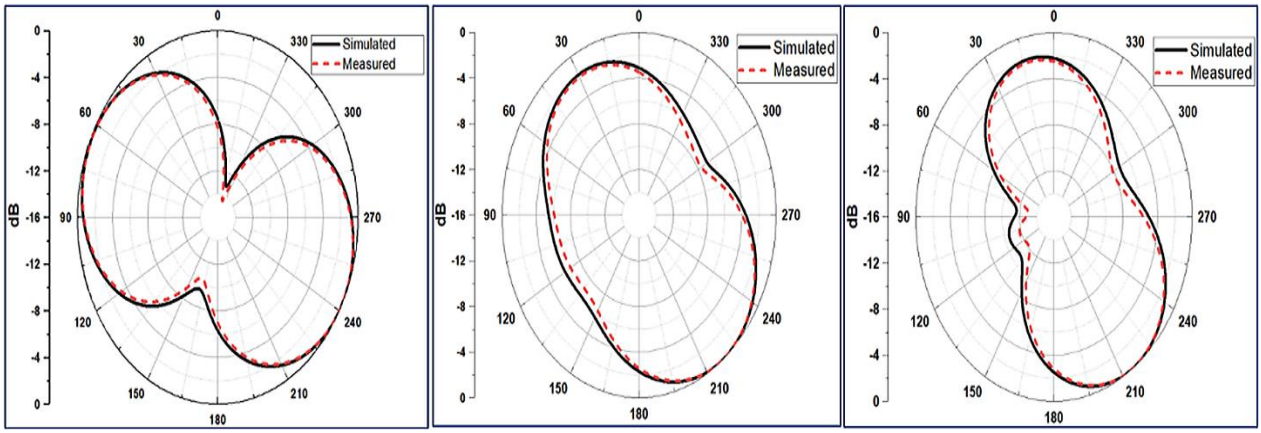


Fig. 7: Anechoic Chamber Measurement set-up for Radiation Patterns of the Delineated Antenna

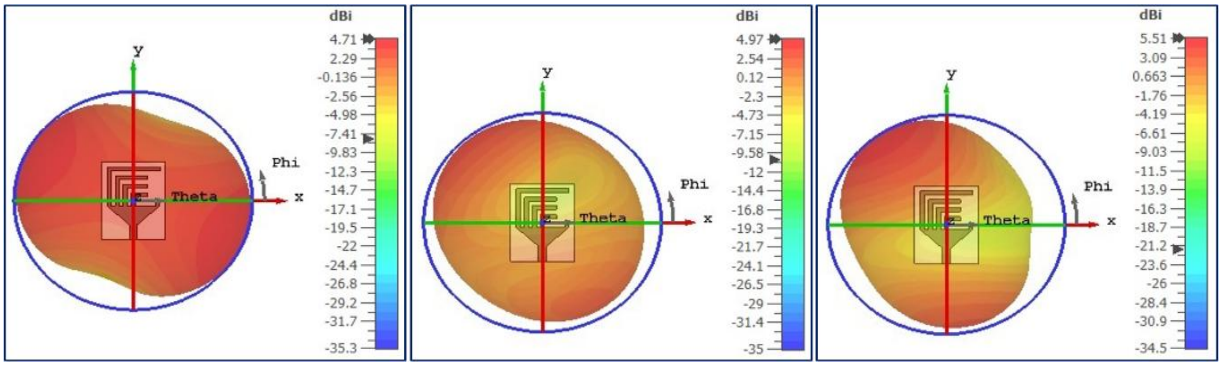
The simulated and measured far-field radiation patterns of the antenna shown in fig 8(a, b, & c) at different resonant frequencies under standard test conditions. The antenna shows almost uniform radiation in the H-plane & two-directional radiation in the E-plane. This behavior provides stable signal coverage in the main directions. The gain and radiation patterns were examined at 4.0, 5.0, and 5.8 GHz, which represent the lower, central, and higher parts of the operating band. The measured results closely matched to simulated ones, confirming the electromagnetic model's accuracy and validating the proposed antenna design's reliability. Minute changes have been similarly linked to both fabrication tolerances and slight alterations in the measurement setup, a phenomenon not exclusive to high-frequency experiments. an antenna demonstrates excellent radiation efficiency over a wide frequencies range, making it highly suitable for various wireless devices uses.



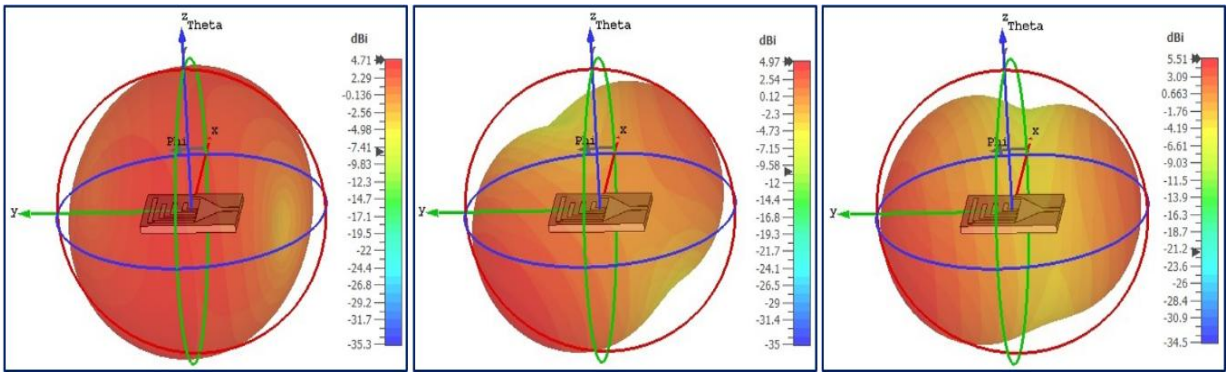
(a) 4.43 GHz **(b) 5.04 GHz** **(c) 5.78 GHz**

Fig. 8: Measured & Simulated Radiation Patterns of the Delineated Antenna at the Resonating Frequencies

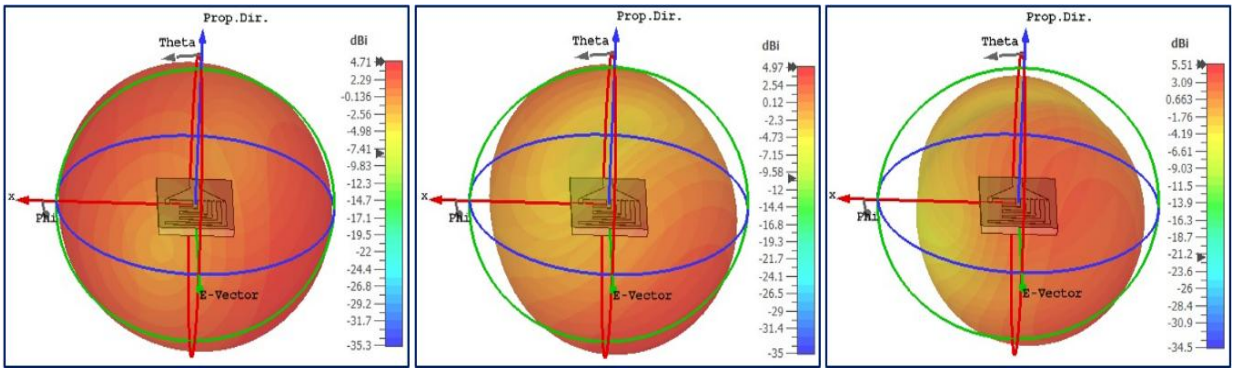
Fig. 9(a, b, & c) depicts the 3D radiation patterns of the antenna at different operating frequencies thereby emphasizing the spatial gain distribution and inherent directional characteristics. The scale of colour, which lies between blue and red, indicates the difference in the intensity of the radiation with the red colour being the loci of the highest gain. The patterns that are observed are isotropic thus allowing an easy transmission of signals in all directions of the azimuth. Therefore, the figure testifies to the high radiation efficiency of an antenna, uniform coverage, and high-quality performance over the given band of operation.



(a) 4.43 GHz



(b) 5.04 GHz

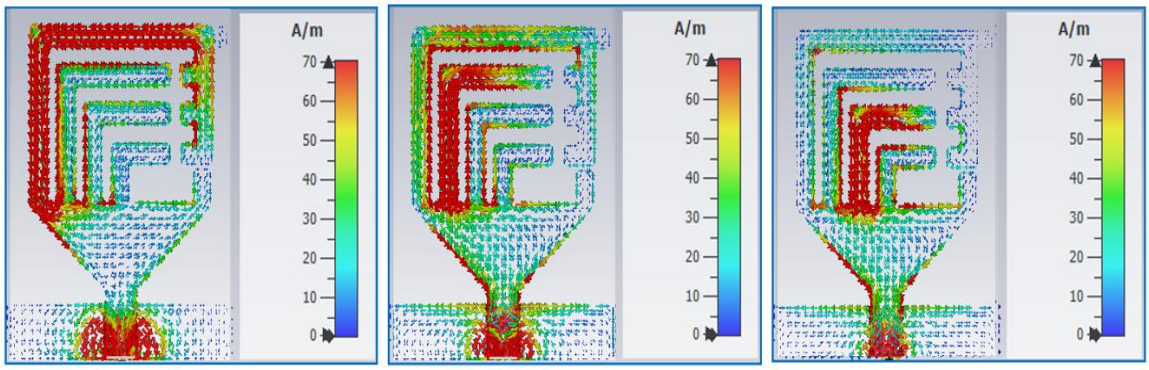


(c) 5.78 GHz

Fig. 9: Simulated 3D Gain Plots of the Proposed Antenna at the Operating Frequencies in the X, Y, and Z Planes

Distribution of Surface Currents of Delineated Antenna

The distribution of currents of a surface of an antenna outlines the main radiating areas as well as clarifies the complexity of the electromagnetic fields in the regions of the radiating devices. The analysis of antenna structures requires a careful analysis of the resonant modes, impedance properties as well as the radiation efficiency of the structure hence giving critical information on the viability of the operation of the antenna structure. The surpassed study of the existing distribution provides the possibility to optimize the design parameters, feeding strategies, and slot geometries and eventually result in the improvement of gain, bandwidth, and polarization purity. As a result, the organized examination of the existing distribution is still invaluable in the strict evaluation and optimization of an antenna performance.



(a) 4.43 GHz **(b) 5.04 GHz** **(c) 5.78 GHz**

Fig. 10: Distribution of Surface Currents of the Delineated Antenna at Operating Frequencies

The diagram in fig. 10 shows how the surface current distributes itself across different resonance frequencies of the proposed antenna. The current path, which moves through the radiating element, becomes visible for observation. The colour scale shows current density levels through its gradient from blue to red. The main current flow of an antenna travels through its feed line before reaching the inner radiating element, which produces radiation. The research discovered various current distribution patterns that appeared during different frequency band tests to prove the system's ability to manage multiple frequency bands and wide frequency ranges. This research deepens the comprehension of the radiation mechanism and validates the antenna's overall effectiveness.

Analysis of Efficiency & Gain

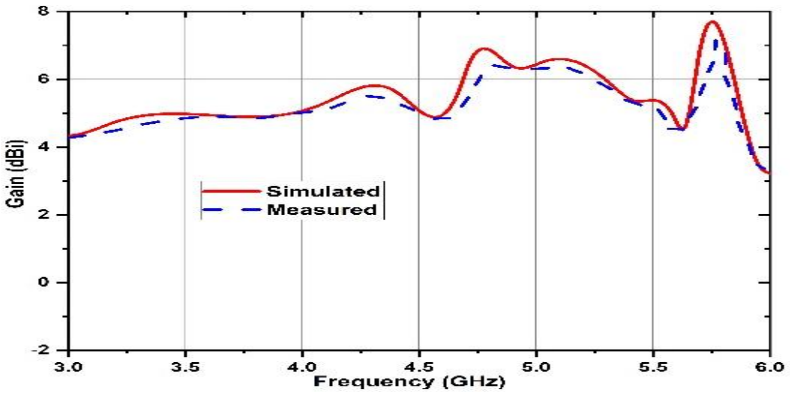
Two-dimensional (2D) gain and radiation efficiency analysis is used to study the radiation behaviour of an antenna in one plane. It shows how an antenna directs energy in different angular regions. From this, the azimuth beamwidth and peak radiation level can be identified. It also includes losses due to absorption and reflection. These parameters are important for evaluating stable operation and overall performance. They also reflect the uniformity of radiation. By improving 2D gain and efficiency, wider coverage and better signal quality can be achieved for future wireless systems.

Gain Computation Method

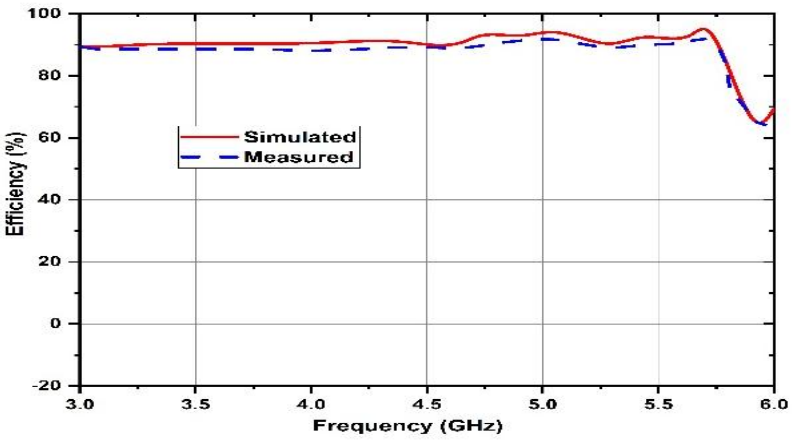
The proposed antenna's realized gain was calculated through the substitution method. Initially, a calibrated horn antenna was placed at the test location, and the received power, Pref, was recorded. Consequently, the horn was swapped out for the antenna under test (AUT) while maintaining identical setup conditions, and the power received, denoted as P_{AUT}, was recorded. Using these recorded values, the gain of the AUT was calculated.

$$G_{AUT}\,(dBi) = G_{ref}\,(dBi) + (P_{AUT} - P_{ref})\ G$$

Here, G_{ref} denotes the known gain of the calibrated reference horn antenna. All measurements were performed using the same transmit power, antenna alignment, cable arrangement, and chamber conditions. This helped in obtaining accurate and repeatable gain values.



(a)



(b)

Fig. 11. Gain and Efficiency Analysis of the Proposed Antenna: (a) Gain vs Freq, (b) Efficiency vs Freq

Fig. 11(a) shows the graph which displays the gain values I achieved between 3 and 6 GHz. The system maintains its frequency stability through all operational frequencies but its gain response shows some small fluctuations. The resonance spectrum shows gain levels which exceed 5 dBi. an antenna exabits its maximum gain of 6.8 dBi during the measurement process which took place at 5.7 GHz. The research data show that the system maintains stable radiation power levels in the tested frequency range. Fig.11(b) presents both the simulated and calculated radiation efficiency over the same 3–6 GHz band. The close trend between them supports the effectiveness of the antenna design. High efficiency has also been observed with the device, and the incident power is retained at around 80 to 90 percent of its original value at the band with a significant decreasing pattern only at frequencies close to 6GHz. The implications of these findings suggest that the antenna will experience minimal electromagnetic energy loss during transmission, which in turn indicates an enhancement in the antenna's overall performance.

Comparison Table

In table 3, the comparison table summarized important parameters of various antenna designs found in the literature, which include frequencies of operation,1 frequency bandwidth, realized gain, efficiency of radiations and size of the antennas. It also explicitly defines improvements, trade-offs and new functionality introduced by the suggested configuration by enabling a first-hand evaluation of the performance of every design. This synthesis provides new insights into the current trends in performance, invents the possibility to advance the field of research, and indicates the gaps in the literature on the topic of the antenna.

Table 3: Comparative Analysis of the Finial Model with Existing Literature

S. No	References	Dimensions (mm^3)	Material	No of Bands	Gain (DBI)	Efficiency (%)
1	Mahendran et al., (2021)	50x30x1.6	FR4	4	2.09	85
2	Sai et al., (2022)	15x24.5x1.6	FR4	2	4.25	90
3	Viswanadha & Raghava, (2021)	10x12x1.524	Polyimide	4	5.81	86
4	Noor et al., (2023)	36x37x1.6	FR4	2	3.83	65
5	Lavadiya et al., (2022)	45x45x1.6	FR4	4	4.56	90
6	Verma et al., (2024)	20x20x1.6	Rogers (5880)	3	4.28	87
7	Abutarboush, (2022)	35x40x0.1	Thick Paper	4	3.12	83
8	El-Hakim & Mohamed, (2023)	40x40x1.6	Rogers (5880)	3	4.86	90
9	Shah et al., (2019)	30x30x1.6	Rogers (5880)	3	3.87	82
10	**Proposed antenna**	**21x16x1.6**	**Rogers (5880)**	**3**	**6.81**	**95**

The prototypes of the antenna are presented in the table that compares all the relevant features, including such characteristics as physical sizes, substrate, frequency ranges of operation, radiative gain, and efficiency. Assemblies on Rogers 5880 and FR4 dielectric patch materials behave differently because of their different values of permittivity. The proposed 21 x 16 x 1.6 mm^3 Rogers 5880 implementation and a 6.81 DBI radiative gain and 95 % of efficiency, thus demonstrating a highly efficient compact design. Thus, the table underscores the importance of meticulously optimizing and selecting materials as essential considerations in the overall functioning of antennas, especially within the multi-band operational spectrum.

Conclusion

The small-scale inverted-L-stub multiband antenna features a Rogers 5880 material to form its 21 x 16 x 1.6 mm^3 dimensions. The design operates with aeronautical mobile telemetry (AMT) systems, Internet-of-Things (IoT) technology, and 5G systems. The system functions at three frequency ranges which include 4.42–4.59 GHz and 5.01–5.90 GHz and 5.74-5.86 GHz. The antenna provides a broad range of impedance bandwidth while keeping its gain steady and producing a stable radiation pattern which remains constant throughout its entire frequency spectrum. The antenna achieves its highest gain of 6.81dBi while maintaining an average radiation efficiency of -83.2 percent which enables separate signal delivery in modern wireless networks. The design achieves successful integration of compact dimensions with wide frequency coverage and high radiation performance which proves its value for upcoming compact communication systems.

Acknowledgements

We Thank the Technical Support from the DST-through S.R./F.ST./E.T. -II./ 2019./ 450. and S.R./ PURSE./2023./196

References

Sai, M. Y., Kavya, S., Bhimavarapu, S. R., Mudaliar, M., & Sharma, S. (2022). CPW fed microstrip patch antenna for dedicated short-range communication. *Wireless Personal Communications*, *122*(4), 3859-3873. https://doi.org/10.1007/s11277-021-09114-7

Li, H., Du, J., Yang, X. X., & Gao, S. (2022). Low-profile all-textile multiband microstrip circular patch antenna for WBAN applications. *IEEE Antennas and Wireless Propagation Letters*, *21*(4), 779-783. https://doi.org/10.1109/LAWP.2022.3146435

Hussain, N., Ghaffar, A., Naqvi, S. I., Iftikhar, A., Anagnostou, D. E., & Tran, H. H. (2022). A conformal frequency reconfigurable antenna with multiband and wideband characteristics. *Sensors*, *22*(7), 2601. https://doi.org/10.3390/s22072601

Mahendran, K., Gayathri, R., & Sudarsan, H. (2021). Design of multi band triangular microstrip patch antenna with triangular split ring resonator for S band, C band and X band applications. *Microprocessors and Microsystems*, *80*, 103400. https://doi.org/10.1016/j.micpro.2020.103400

Shah, S. A. A., Shah, I. A., Hayat, S., & Yoo, H. (2024). Ultra-miniaturized implantable antenna enabling multiband operation for diverse industrial IoMT devices. *IEEE Transactions on Antennas and Propagation*, *72*(2), 1352-1362. https://doi.org/10.1109/TAP.2024.3349782

Samal, P. B., Chen, S. J., & Fumeaux, C. (2022). Wearable textile multiband antenna for WBAN applications. *IEEE Transactions on Antennas and Propagation*, *71*(2), 1391-1402. https://doi.org/10.1109/TAP.2022.3230550

Rana, S., Kumar, A., Mohan, A., Kanaujia, B. K., & Matekovits, L. (2024). A planar wideband antenna for full duplex communication with significant peak gain. *IEEE Access*, *12*, 153181-153187. https://doi.org/10.1109/ACCESS.2024.3478803

Ranjan, P., & Kumar, A. (2021). Circularly polarized ultra–wide band filtering antenna with controllable band-notch for wireless communication system. *AEU-International Journal of Electronics and Communications*, *135*, 153738. https://doi.org/10.1016/j.aeue.2021.153738

Angadi, S., Viswanadha, K., Chinthaginjala, R., & Tai-Hoon, K. (2024). Meta-atom loaded circularly polarized triple band patch antenna for Wi-Fi, ISM and X-band communications. *Heliyon*, *10*(7). https://doi.org/10.1016/j.heliyon.2024.e28906

Viswanadha, K., & Raghava, N. S. (2021). Design and analysis of a dual-polarization multiband oval ring patch antenna with L-stubs and folded meander line for C-band/X-band/Ku-band/K-band communications. *International Journal of Electronics*, *108*(4), 647-663. https://doi.org/10.1080/00207217.2020.1793411

Kumar, L., Nath, V., & Reddy, B. V. R. (2023). Triple-band stub loaded patch antenna with high gain for 5G Sub-6 GHz, WLAN and WiMAX applications using DGS. *Facta Universitatis, Series: Electronics and Energetics*, *36*(2), 171-188. https://doi.org/10.2298/FUEE2302171K

Khan, K. A., & Nokerov, S. M. (2021). Optimization of multi-band characteristics in fan-stub shaped patch antenna for LTE (CBRS) and WLAN bands. *Proceedings of Engineering and Technology Innovation*, *18*, 25. https://doi.org/10.46604/peti.2021.6713

Chung, M. A., Lee, M. C., Hsu, C. C., & Lin, C. W. (2024). Multi-band coupled-fed antenna for 4G LTE, sub-6G, and WLAN frequency bands in various electronic devices. *IEEE Access*, *12*, 45398-45422. https://doi.org/10.1109/ACCESS.2024.3380620

Noor, S. K., Jusoh, M., Sabapathy, T., Rambe, A. H., Vettikalladi, H., M. Albishi, A., & Himdi, M. (2023). A patch antenna with enhanced gain and bandwidth for sub-6 GHz and sub-7 GHz 5G wireless applications. *Electronics*, *12*(12), 2555. https://doi.org/10.3390/electronics12122555

Faris, A. S., & Tulu, M. M. (2024). Design and Performance Analysis of Multi-band Antenna for 5G Application. *Wireless Personal Communications*, *136*(1), 429. https://doi.org/10.1007/s11277-024-11279-w

Lavadiya, S. P., Sorathiya, V., Kanzariya, S., Chavda, B., Naweed, A., Faragallah, O. S., ... & Rashed, A. N. Z. (2022). Low profile multiband microstrip patch antenna with frequency reconfigurable feature using PIN diode for S, C, X, and Ku band applications. *International journal of communication systems*, *35*(9), e5141. https://doi.org/10.1002/dac.5141

Kaur, A., & Malik, P. K. (2021). Multiband Elliptical Patch Fractal and Defected Ground Structures Microstrip Patch Antenna for Wireless Applications. *Progress In Electromagnetics Research B*, *91, 157-173*. http://dx.doi.org/10.2528/PIERB20102704

Wa'il, A., Shaaban, R. M., & Duffy, A. P. (2022). Design, simulation, and fabrication of a double annular ring microstrip antenna based on gaps with multiband feature. *Engineering Science and Technology, an International Journal*, *29*, 101033. https://doi.org/10.1016/j.jestch.2021.06.013

Verma, R. K., Kumar, A., Pattanayak, P., Rajpoot, V., Bali, V., & Mathur, S. (2024). Design and analysis of multiband microstrip antenna using multiple notches for wireless communication in L and S-band applications. *Wireless Personal Communications*, *137*(4), 2199-2216. https://doi.org/10.1007/s11277-024-11482-9

Sharma, U., Srivastava, G., Khandelwal, M. K., & Roges, R. (2024). Design Challenges and Solutions of Multiband MIMO Antenna for 5G/6G Wireless Applications: A Comprehensive Review. *Progress in Electromagnetics Research B*, *104*.http://dx.doi.org/10.2528/PIERB23101904

Abutarboush, H. F. (2022). Silver nanoparticle inkjet-printed multiband antenna on synthetic paper material for flexible devices. *Alexandria Engineering Journal*, *61*(8), 6349-6355. https://doi.org/10.1016/j.aej.2021.11.060

El-Hakim, H., & Mohamed, H. A. (2023). synthesis of a multiband microstrip patch antenna for 5G wireless communications. *Journal of Infrared, Millimeter, and Terahertz Waves*, *44*(9), 752-768. https://doi.org/10.1007/s10762-023-00937-y

Wang, L., Yu, J., Xie, T., & Bi, K. (2021). A novel multiband fractal antenna for wireless application. *International Journal of Antennas and Propagation*, *2021*(1), 9926753. https://doi.org/10.1155/2021/9926753

Shah, I. A., Zada, M., & Yoo, H. (2019). Design and analysis of a compact-sized multiband spiral-shaped implantable antenna for scalp implantable and leadless pacemaker systems. *IEEE Transactions on Antennas and Propagation*, *67*(6), 4230-4234. https://doi.org/10.1109/TAP.2019.2908252

Rajkumar, R., & Kommuri, U. K. (2018). A triangular complementary split ring resonator based compact metamaterial antenna for multiband operation. *Wireless Personal Communications*, *101*(2), 1075-1089. https://doi.org/10.1007/s11277-018-5749-7